Title

Atomic Basis for the Species-specific Inhibition of αV Integrins by Monoclonal Antibody 17E6 Is Revealed by the Crystal Structure of αVβ3 Ectodomain-17E6 Fab Complex*

Journal

Journal of Biological Chemistry, 289(20)

ISSN

0021-9258

Authors

Mahalingam, Bhuvaneshwari
Van Agthoven, Johannes F
Xiong, Jian-Ping
et al.

Publication Date

2014-05-01

DOI

10.1074/jbc.m113.546929

THE JOURNAL OF BIOLOGICAL CHEMISTRY VOL. 289, NO. 20, pp. 13801–13809, May 16, 2014

Atomic Basis for the Species-specific Inhibition of αV Integrins by Monoclonal Antibody 17E6 Is Revealed by the Crystal Structure of αVβ3 Ectodomain-17E6 Fab Complex*

Received for publication, December 30, 2013, and in revised form, February 26, 2014 Published, JBC Papers in Press, April 1, 2014, DOI 10.1074/jbc.M113.546929

Bhuvaneshwari Mahalingam[‡], Johannes F. Van Agthoven[‡], Jian-Ping Xiong[‡], José Luis Alonso[§], Brian D. Adair[‡], Xianliang Rui[§], Saurabh Anand[§], Mehrdad Mehrbod[¶], Mohammad R. K. Mofrad[¶], Christa Burger[‖], Simon L. Goodman[**‡‡], and M. Amin Arnaout[‡§1]**

From the [‡]Structural Biology Program and the [§]Leukocyte Biology and Inflammation Program, Departments of Medicine and Developmental & Regenerative Biology, Massachusetts General Hospital and Harvard Medical School, Charlestown, Massachusetts 02129, the [¶]Departments of Bioengineering and Mechanical Engineering, University of California, Berkeley, California 94720, [**]Merck KGaA and [‖]Discovery Technologies, Molecular Pharmacology, and [‡‡]Therapeutic Innovation Platform, Oncology, Darmstadt 64271, Germany

Background: 17E6, a primate-specific mouse mAb that inhibits αV integrins, is in phase II trials for treating cancer.
Results: We determined crystal structure of the αVβ3–17E6 Fab complex, revealing the molecular basis of 17E6 specificity and function.
Conclusion: 17E6 is an allosteric inhibitor of fibronectin-integrin interaction.
Significance: The defined 17E6 epitope may help in developing novel therapeutics targeting related regions in other integrins.

The function-blocking, non-RGD-containing, and primate-specific mouse monoclonal antibody 17E6 binds the αV subfamily of integrins. 17E6 is currently in phase II clinical trials for treating cancer. To elucidate the structural basis of recognition and the molecular mechanism of inhibition, we crystallized αVβ3 ectodomain in complex with the Fab fragment of 17E6. Protein crystals grew in presence of the activating cation Mn^{2+}. The integrin in the complex and in solution assumed the genu-flected conformation. 17E6 Fab bound exclusively to the Propeller domain of the αV subunit. At the core of αV-Fab interface were interactions involving Propeller residues Lys-203 and Gln-145, with the latter accounting for primate specificity. The Propeller residue Asp-150, which normally coordinates Arg of the ligand Arg-Gly-Asp motif, formed contacts with Arg-54 of the Fab that were expected to reduce soluble FN10 binding to cellular αVβ3 complexed with 17E6. This was confirmed in direct binding studies, suggesting that 17E6 is an allosteric inhibitor of αV integrins.

Integrins are α/β heterodimeric adhesion receptors that transmit biochemical and mechanical signals bidirectionally across the plasma membrane, thus serving as key communication molecules between the extracellular environment and the cytoskeleton (1). The α and β subunits associate noncovalently into a ligand-binding "head" segment, comprising a β-Propeller domain from the α-subunit and a von Willebrand Factor A type (vWFA) domain (βA or I-like) from the β-subunit. The head segment sits on top of two leg-like extensions, each possessing a single-pass transmembrane helix, which anchors the receptor to the plasma membrane, followed by two short cytoplasmic C-terminal tails (2). Integrin function is tightly regulated: integrins are normally kept in an inactive state (unable to bind soluble physiologic ligands), thus allowing, for example, leukocytes and platelets to circulate in the blood without aggregation or adhesion to the vessel walls. Physiologic stimuli, acting through the short integrin α/β cytoplasmic tails, induce allosteric changes in the ectodomain that switch it to a high affinity state, capable of binding soluble ligand, (so called "inside-out" activation) (2). Bound ligand then induces structural rearrangements in the ectodomain, forging links via the β cytoplasmic tail, with the actin cytoskeleton (3). This "outside-in" signaling can be enhanced by lateral clustering of integrins induced by multivalent ligand (4). This promotes the assembly of cytoskeletal and signaling molecular complexes at "focal adhesions," regulatory sites through which forces can be applied on liganded integrins through the cytoskeleton or extracellularly through ECM stiffening or shear stress (2). Inappropriate integrin activation contributes to the pathogenesis of many diseases including cancer growth and metastasis (1, 5).

The integrin αV subunit is in five integrins (αVβ1, αVβ3, αVβ5, αVβ6, and αVβ8). This subfamily exclusively recognizes the tripeptide sequence Arg-Gly-Asp (RGD) in ligands that include fibronectin, vitronectin, fibrinogen, and osteopontin (5). αVβ3, the most extensively studied member of this subfamily, is up-regulated in angiogenic endothelium (6) and on several tumor cell types including glioma (7, 8) and melanoma (9) where it supports invasion and metastasis (5), making αVβ3 an attractive therapeutic target.

* This work was supported, in whole or in part, by National Institutes of Health Grants DK088327, DK096334, and DK007540 (to M. A. A.). This work was also supported by National Science Foundation CAREER Award CBET-0955291 (to M. R. K. M.).

The atomic coordinates and structure factors (code 4O02) have been deposited in the Protein Data Bank (http://wwpdb.org/).

[1] To whom correspondence should be addressed: Massachusetts General Hospital, 149 13th St., Charlestown, MA 02129. Tel.: 617-726-5663; E-mail: aarnaout1@mgh.harvard.edu.

The αV-specific mAb 17E6 as IgG or $F(ab')_2$ inhibits cell attachment and spreading of cancer cells *in vitro* and *in vivo* and induces cell detachment (10, 11), suggesting that it disrupts stable αV-ligand interactions (10). Cellular αVβ3 that is dimerized by bound IgG or $F(ab')_2$, forms of 17E6, but not by anti-αVβ3 mAbs 2E7 (nonblocking anti-αV) or AP3 (nonblocking anti-β3), is internalized (12), which may contribute to its inhibitory effects on cell adhesion, and links the 17E6 epitope to adhesion reversal. Although the primary sequence of the αV chain is strongly conserved between species, 17E6 does not bind murine αV integrins.

To explore the structural basis of its specificity and function, we crystallized the complex of the Fab fragment of 17E6 with the αVβ3 ectodomain (13) in the presence of the activating metal ion Mn^{2+}. The new structure assumed a bent conformation, exhibited some flexibility at the α-genu, revealed the structural basis for 17E6 selectivity to the αV subunit of primates, and defined the antibody-integrin binding interface. The significance of these findings is discussed.

EXPERIMENTAL PROCEDURES

Reagents and Site-directed Mutagenesis—Restriction and modification enzymes were obtained from New England Biolabs, Invitrogen, or Fisher Scientific. All cell culture reagents were obtained from Invitrogen. Purified αVβ3 was generated and purified as described (13). The noninhibitory mAb AP3 (ATCC) detects the β3-subunit in all conformations. The Fab fragment of the αV-specific mAb 17E6 (10) generated by papain digestion was verified by SDS-PAGE. The Fab fragment of the function-blocking mAb 7E3, which binds to the βA domain of the β3 subunit (14) was purchased (Eli Lilly and Company, Indianapolis, IN). Wild-type human FN9–10 and FN10[2] were produced as described (15). Lys-203 → Ala (K203A) substitution in human αV and Lys-145 → Asn → Gln-145 → Asp (K145N/Q145D) substitution in mouse αV were generated by PCR and confirmed by DNA sequencing.

The adherent cell lines Vero, COS-7, and CV-1 (monkey), C6 and Rat-1 (rat), EBTr (bovine), CRFK (cat), MDCK (dog), GeLu (gerbil), CGBQ (goose), JH4 (guinea pig), BHK-21 and CS-1B3 (hamster), E. Derm (horse), MPK (mini-pig), QT6 (quail), SIRC (rabbit), and PL-1 Ut (raccoon) were obtained from ATCC and cultured as recommended by ATCC. B16-F10 (mouse) was from the late Dr. J. Folkman (Childrens Hospital, Boston, MA), and WM164 was from Dr. M. Herlyn (Wistar Institute, Philadelphia, PA); both were cultured in DMEM plus 10% FCS. CS-1B3 was from Dr. D. Cheresh (University California, San Diego, CA) and was cultured in RPMI plus 10% FCS, 1 mM sodium pyruvate, and 500 μg/ml G418.

Cell Adhesion Inhibition Assays—Cells were allowed to adhere for 1 h at 37 °C on vitronectin-coated surfaces in the presence of serially diluted 17E6 or cilengitide as described elsewhere (10). Cilengitide is an RGD-containing inhibitor of αVβ3 and αVβ5 integrins (16).

Formation of αVβ3–17E6 Fab Complex—αVβ3 ectodomain (at 5–10 mg/ml) was mixed with a ~4-fold molar excess of 17E6 Fab in 20 mM HEPES buffer, pH 7.5, containing 5 mM $CaCl_2$, incubated for 30 min at 4 °C, and then chromatographed in the same buffer (Superdex S-200; GE Healthcare). Fractions from the peak containing complexes were collected as previously described (15, 17), pooled, and concentrated (to 8–10 mg/ml).

Crystallography, Structure Determination, and Refinement—The αVβ3–17E6 Fab complex was crystallized at room temperature by vapor diffusion using the hanging drop method. Data were collected from crystals obtained using a reservoir solution comprising sodium citrate buffer, pH 5.6, 13.5% PEG, 10 mM $MnCl_2$, 1% glycerol, 90 mM trimethylamine *N*-oxide, and 0.3 M sodium nitrate. Crystals were frozen in liquid nitrogen. Glycerol was used as a cryoprotectant, and its concentration in the reservoir solution was increased to 23% in 2% steps. The data were collected at Beamline 19ID at Advanced Photon Source (APS) (Chicago, IL) and were processed using the HKL package (18). The asymmetric unit contained one molecule of the complex. Molecular replacement using Phaser (19) was used for structure determination. Structures of αVβ3 (Protein Data Bank code 1jv2) and Fab from Protein Data Bank code 2vdl were used as starting models for molecular replacement. Refinement was performed using the deformable elastic network procedure for low resolution data (20) in the CNS (21). This was followed by refinement in 1.8.4 version of PHENIX (22) using Protein Data Bank structures 3ije and Fab from 2vdl as reference models, Translation/Liberation/Screw (TLS), positional, and individual temperature factors. In addition to the default restraints, automatic optimization of x-ray and stereochemistry/ADP and additional Ramachandran restraints were used in the last cycles. Model building was performed initially using O (23) and later using Coot (24). Structural illustrations were prepared with the Chimera software (25).

EM and Imaging Studies—The αVβ3–17E6 complex was applied to glow-discharged continuous carbon grids, rapidly washed in water, and stained with 0.75% uranyl formate. Grids were imaged on a Philips CM10 electron microscope (100 kV; nominal magnification, 41,000×; defocus range, −1.0 to −1.8 μm). Images were recorded on SO163 film (Kodak) and digitized with a step size of 6.35 μm (Nikon Coolscan 8000). Images were subjected to 2-fold pixel averaging to yield 2.76 Å/pixel at the image. Image processing was performed with the EMAN suite (26). 2,530 particles were selected and Contrast Transfer Function (CTF) phase-corrected. Selected particles were subjected to an initial reference-free alignment and averaging and k-means classification using 10 classes. Class averages were refined with seven rounds of multireference classification using the class averages as references as described (27).

mAb Binding to Wild-type and Mutant Cellular αVβ3—HEK 293T cells were co-transfected with a plasmid encoding full-length human WT β3 and pcDNA3 plasmids encoding WT or K203A-mutated αV, together with Lipofectamine 2000 (Invitrogen) according to the manufacturer's specifications. 48 h after transfection, cells were detached (10 mM EDTA/PBS), washed two times in Hanks' balanced saline solution (HBSS) and once in HBSS containing 1 mM $CaCl_2$/1 mM $MgCl_2$ ($HBSS^{2+}$). 6×10^5 cells in 100 μl of $HBSS^{2+}$ were stained with the Fab fragments of 17E6 or 7E3 (10 μg/ml; 30 min; 4 °C), followed by one wash, and then addition of FITC-labeled anti-

[2] The abbreviations used are: FN, fibronectin; HBSS, Hanks' balanced salt solution.

mouse Fab (20 μg/ml; 30 min; in the dark; 4 °C). Samples were again washed once and then fixed (1% buffered paraformaldehyde). To assess expression levels, 6×10^5 cells in 100 μl of $HBSS^{2+}$ were incubated with AP3 mAb (10 μg/ml; 30 min; 4 °C), washed and then stained with allophycocyanin-labeled anti-mouse IgG (20 μg/ml). 20,000 cells were analyzed for each sample using a FACSCalibur flow cytometer (BD Biosciences, San Jose, CA). Binding of 17E6 or 7E3 to αVβ3-expressing HEK293T was expressed as mean fluorescence intensity, as determined using the CellQuest software (BD Biosciences), and normalized by dividing this mean fluorescence intensity by the mean fluorescence intensity for AP3 binding to WT αVβ3 and multiplying by 100.

To assess the effect of mouse to human K145N/Q145D αV chimera on 17E6 binding to mouse αV-integrin, murine Flip-In-3T3 cells (Invitrogen) were transfected with Flip-In pcDNA5/FRT plasmids encoding mouse or human WT αV subunits or mouse αV containing the K145N → Q145D mutant αV. Transfected cells were enriched for 17E6 binding by selecting for adherent cells in each of two rounds of panning on 17E6 coated surfaces. After harvesting (10 mM EDTA/PBS), 1×10^6 transfected cells in 100 μl of DPBS (Invitrogen) containing 1 mM $CaCl_2$/1 mM $MgCl_2$ and 1% BSA were incubated with 17E6 IgG (10 μg/ml) in a total volume of 0.5 ml for 30–60 min on ice, washed, and then stained with FITC-labeled goat anti mouse IgG (BD Biosciences) for 30 min on ice. After washing, the viable cells were analyzed by flow cytometry.

Ligand Binding Assays—K562 cells (American Type Culture) stably expressing αVβ3 (K562-αVβ3) were generated as described (28) and maintained in Iscove's modified Dulbecco's medium supplemented with 10% heat-inactivated fetal bovine serum, 50 IU/ml penicillin and streptomycin, and 0.5–1.0 mg/ml G418. For ligand binding experiments, cells were harvested and washed two times in HEPES-buffered saline containing 1% BSA and 10 mM glucose (HBG buffer). 1 mM $CaCl_2$ with 1 mM $MgCl_2$ or 1 mM $MnCl_2$ were added to 6×10^5 cells in 100 μl of HBG buffer and incubated in the presence or absence of a saturating amount of unlabeled 17E6 Fab (30 μg/ml for 30 min at 20 °C), washed once in HBSS buffer containing the corresponding metal ion, and then incubated with Alexa Fluor 488-labeled wild-type FN10 or FN9–10 (2.5 μg/ml for 30 min in the dark). Cells were washed once in HBSS containing the corresponding ions, fixed (1% buffered paraformaldehyde), and analyzed by flow cytometry.

Molecular Dynamics Simulations—All atom simulations of αV Propeller domain and 17E6 Fab were performed with the program NAMD, using a CHARMM27 force field (29–31). The temperature and pressure of the system were held constant at 310 K and 1 atm, respectively, using the Langevin's piston and Hoover's method, as successfully used previously for modeling integrins (29–32). The time step was taken as 2 fs. The cutoff distance for nonbonded interactions was 1.2 nm, and the particle mesh Ewald method was used for electrostatic force calculations (29). Hydrogen atom bond length was constrained using SHAKE (33). All systems were minimized, at 20,000 steps, and equilibrated for 40 ns.

Interactions were simulated using the crystal structure of αVβ3–17E6 Fab complex. Q145D/K145N and K203A mutations were made in the Propeller structure using the software Swiss-Pdb Viewer 4.1.0 (34). The Propeller and Fab molecules were shifted by ~1 Å from their original bound state to compare the effects of the mutations. Each of the three systems was solvated in a water box of 188 × 127 × 139 Å in size and ionized with 150 mM NaCl to represent the solvent.

The association constant (k_a) of Propeller-Fab interaction was calculated according to Equation 1,

$$k_a = e^{\frac{-\Delta G}{k_B T}} \quad \text{(Eq. 1)}$$

where ΔG, k_B, and T are the free energy of association per mole, Boltzmann constant, and temperature, respectively. Gibbs free energy was calculated according to Equation 2,

$$G = U + PV - TS \quad \text{(Eq. 2)}$$

where U, P, V, S, and T are the interaction energy, pressure, volume, entropy, and temperature (at 310 K), respectively. Interaction energy was computed as the sum of the electrostatic and van der Waals energies. The ratio of k_a for mutant to that of wild-type structure was derived according to Equation 3.

$$\frac{k_{a-\mathrm{mu}}}{k_{a-\mathrm{wt}}} \cong \frac{e^{\frac{-\Delta U_{\mathrm{mu}} + T \cdot \Delta S_{mu}}{k_B T}}}{e^{\frac{-\Delta U_{\mathrm{wt}} + T \cdot \Delta S_{\mathrm{wt}}}{k_B T}}} \cong e^{\frac{-\Delta U_{\mathrm{mu}} + \Delta U_{\mathrm{wt}}}{k_B T}} \quad \text{(Eq. 3)}$$

RESULTS

17E6 Only Inhibits Primate αV Integrins—Established adherent cell lines were examined for sensitivity to 17E6 in cell adhesion-inhibition assays on the αVβ3/αVβ5 integrin ligand vitronectin. Of 18 species tested (primates to avians), only cells from human and monkey were inhibited by 17E6 (IC_{50} = 0.13–1.3 nM). IC_{50} was not attained up to 300 nM with cells from any other species. This was not due to lack of integrin expression, because the attachment to vitronectin of cells from every species was specifically inhibited by the αVβ3/αVβ5 peptidic inhibitor cilengitide with IC_{50} scattered at ~1 μM (16, 35) (Table 1 and Fig. 1). We investigated the structural basis for this specificity.

Crystal Structure of Fab in Complex with αVβ3 Ectodomain—The water-soluble ectodomain of αVβ3 (13) formed a stable complex with the Fab fragment of 17E6, and the complex was crystallized in presence of the integrin activating metal ion Mn^{2+}. We determined the crystal structure of the αVβ3–17E6 Fab complex by molecular replacement and refined the model with data to 3.6Å resolution. The structure contained one integrin-Fab complex in the asymmetric unit, consisting of αV residues (Phe-1 to Ile-833 and Leu-872 to Trp-953), and β3 residues Gly-1 to Cys-687, Fab heavy chain residues Gln-1 to Arg-218 and light chain residues Asp-1 to Cys-214 (Fig. 2*A*). The four metal ion sites at the base of the Propeller and at ADMIDAS of βA were occupied, but no metal ion density was present at MIDAS, LIMBS, or at the α-genu. Crystallographic data and refinement statistics are given in Table 2. αVβ3 in complex with 17E6 Fab assumed a bent conformation. EM class averages of 17E6-bound αVβ3 segregated into two different orientations (Fig. 2*B*) and showed that the integrin also

TABLE 1
Species-specific inhibition of cell adhesion by 17E6

Cell line[a]	Species	IC_{50} 17E6	IC_{50} Cilengitide
		nM	*μM*
WM164	Human	0.26	4
Vero	Monkey	1.3	~20
COS 7	Monkey	0.13	0.2
CV-1	Monkey	0.19	0.4
C6	Rat	>300	0.4
Rat 1	Rat	>300	2
EBTr	Bovine	>300	9
CRFK	Cat	>300	0.4
MDCK	Dog	>300	2
Duck embryo	Duck	>300	5
GeLu	Gerbil	>300	3.5
CGBQ	Goose	>300	0.8
JH4	Guinea pig	>300	0.4
BHK-21	Hamster	>300	0.4
CS-1B3	Hamster	>300	0.4
E.Derm	Horse	>300	4
MPK	Mini pig	>300	0.08
Mv 1 Lu	Mink	>300	0.1
B16-F10	Mouse	>300	2
QT6	Quail	>300	0.2
SIRC	Rabbit	>300	0.7
PL 1 Ut	Raccoon	>300	1

[a] From 18 species, 22 cell lines were allowed to attach to vitronectin-coated surfaces in the presence of serially diluted 17E6 or cilengitide. Only the attachment of human- and monkey-derived cell lines was inhibited by 17E6. All species were inhibited by cilengitide.

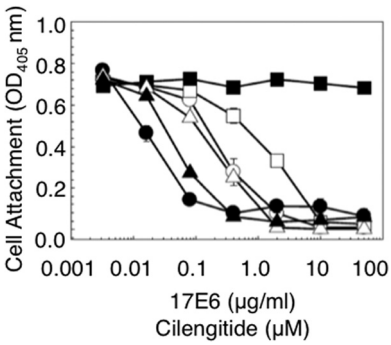

FIGURE 1. **Species-dependent inhibition of cell attachment by 17E6 and species-independent inhibition by cilengitide.** Representative cell adhesion inhibition assay comparing human melanoma cell line WM164 (*circles*), monkey cell line CV-1 (*triangles*), and rat cell line Rat-1 (*squares*). *Filled symbols* show response to 17E6, and *open symbols* show response to the RGD-peptide cilengitide. Human and monkey cells are inhibited, and rat cells are not affected by 17E6. Each species is inhibited by cilengitide.

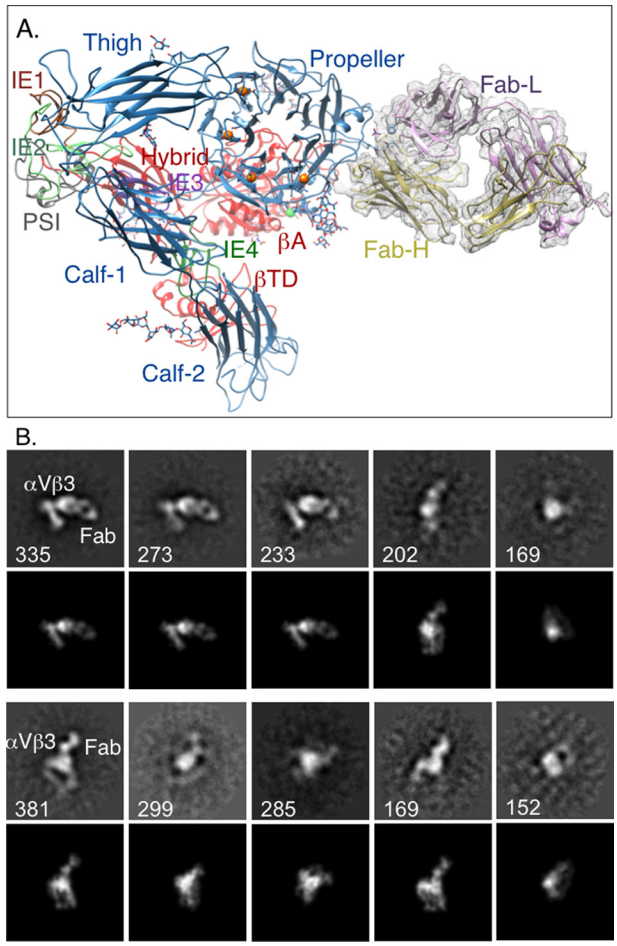

FIGURE 2. **Structure of αVβ3–17E6 Fab complex.** *A*, ribbon diagram of αVβ3 bound to 17E6 Fab. αV subunit is in *steel blue*, and β3 subunit domains (in different colors for better visualization) are labeled, as are the heavy and light chains of 17E6 Fab (Fab-H and Fab-L, respectively). The four metal ions of the Propeller domain (*orange spheres*) and βA ADMIDAS (*green*) are shown. No metal ions are seen at the α-genu, MIDAS, or LIMBS. Glycan carbons are shown in the respective domain color with oxygens and nitrogens colored *red* and *blue*, respectively. Sigma-weighted $2F_o - F_c$ map for the Fab is shown contoured at 1.0 σ. *B*, EM structure of 17E6-Fab-bound αVβ3. All 10 class averages of αVβ3 ectodomain displaying bound 17E6 Fab with particle numbers are shown in the *first* and *third rows*. Averages were generated from 2,530 particles. The corresponding projections of the model crystal structure (shown in Fig. 2*A*) are shown in the *second* and *fourth rows*, respectively. The length of each box side is 353 Å. Two different orientations are observed, both clearly indicating a bent conformation with 17E6 bound as seen in the crystal structure.

assumed a bent conformation when adsorbed from solution, thus complementing the crystallographic data.

Interactions between αVβ3 and 17E6 Fab—17E6 Fab only contacted the αV subunit of the integrin heterodimer and did so primarily through its heavy chain. The three heavy chain CDRs (CDR_{H1-3}) contacted loop residues in blades 2 and 3 of the αV Propeller domain (Fig. 3*A*). Core interactions involved Gln-145 and Lys-203 from D2A3 loop and D3 strand of the Propeller domain, respectively, which inserted into adjacent hydrophobic pockets in the heavy chain (Fig. 3*B*). NE2 of Gln-145 H-bonded with carbonyl oxygens of Phe-99_{H3} and Leu-100_{H3}; its OE1 H-bonded to the main chain amide of Trp-33_{H1} and the carbonyl oxygen of Phe-99_{H3}. The main chain amide and carbonyl oxygen of Gln-145, respectively, formed H-bonds with the carbonyl oxygen of Ser-31_{H1} and NE1 of Trp-33_{H1}. The side chain NZ of Lys-203 formed a bidentate salt bridge with Asp-106_{H3}. In addition, Tyr-200 formed a H-bond with NH_2 of Arg-102_{H3}, and the carbonyl oxygen of Asn-198 hydrogen-bonded with Nε and NH_2 of Arg-102_{H3}. Asp-146 contacted Arg-54_{H2}, and Asp-150 made a salt bridge with Arg-54_{H2}, and its carbonyl oxygen H-bonded to NH1 of Arg-54_{H2}.

Atomic Basis for Specificity of mAb17E6 for Primate αVβ3—Sequence analysis of the species tested in cell adhesion-inhibition assays (Table 1) revealed that every species other than humans and macaque lacked Gln-145 → Asp and expressed Lys-145 → Asn or in avians Thr-Thr at this site (Fig. 4). By contrast Lys-203 was conserved across species (Fig. 4). Replacing Lys-145 → Asn with Gln-145 → Asp in mouse αV and expressing this chimeric αV with the endogenous mouse β-chains in 3T3 cells imparted reactivity of 17E6 with the chimeric mouse cell surface receptor to essentially the same level as full-length human αV (Fig. 5*A*). The importance of the con-

TABLE 2
Data collection and refinement statistics

	αVβ3-17e6
Data collection	
Beamline	ID19 at APS
Space group	P21212
Unit cell dimensions (Å; °)	$\alpha = 110.5$, $\beta = 267.0$, $c = 102.2$; $\alpha = \beta = \gamma = 90$
Resolution range (Å)	50–3.6
Wavelength (Å)	0.97857
Total reflections	568,528
Unique reflections	31,351 (1,931)[a]
Completeness	87.9 (55.2)
Redundancy	3.8 (2.8)
Molecules in asymmetric unit	1
Average I/σ	8.3 (1.0)
R_{sym} (%)	13.1 (86.6)
Wilson B-factor	112.7
Refinement statistics	
Resolution range (Å)	49.9–3.6
R_{factor} (%)	25.5 (31.3)
R_{free} (%)[b]	31.0 (35.4)
No. of atoms	
Protein residues	2,069
NO_3	2
Average B-factor	172.4
Root mean square deviations	
Bond lengths (Å)	0.005
Bond angles (°)	0.99
Ramachandran plot	
Most favored (%)	83.0
Allowed regions (%)	13.0
Outliers (%)	4.0
Clash score (%)	9.84

[a] The values in parentheses are for the highest resolution shell (0.1 Å).
[b] R_{free} was calculated with 5% of the data.

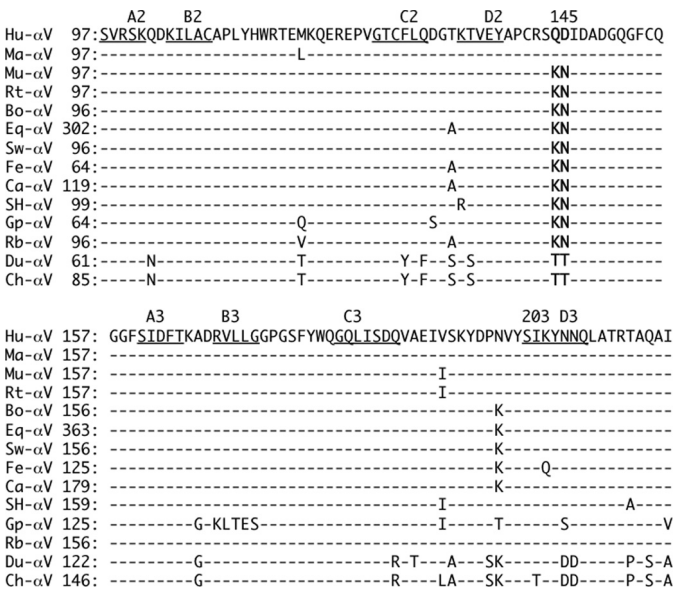

FIGURE 4. **Sequence alignment of 17E6 binding regions of αV integrins from multiple species.** Shown is the sequence alignment of the αV integrin sequences from the four-strand blades 2 and 3 (strands A–D *underlined*) of the Propeller (Ser-97 to Ile-216 of the human sequence) from 14 of the 18 species analyzed for sensitivity to 17E6. Sequences used were from GenBank™ translations of human (*Hu*), macaque (*Ma*), mouse (*Mu*), rat (*Rt*), bovine (*Bo*), horse (*Eq*), pig (*Sw*), cat (*Fe*), dog (*Ca*), Syrian hamster (*SH*), guinea pig (*Gp*), rabbit (*Rb*), duck (*Du*), and chicken (*Ch*). Divergence from the human consensus sequence is shown. The divergent species-specifying site Gln-145 Asp is in *bold*.

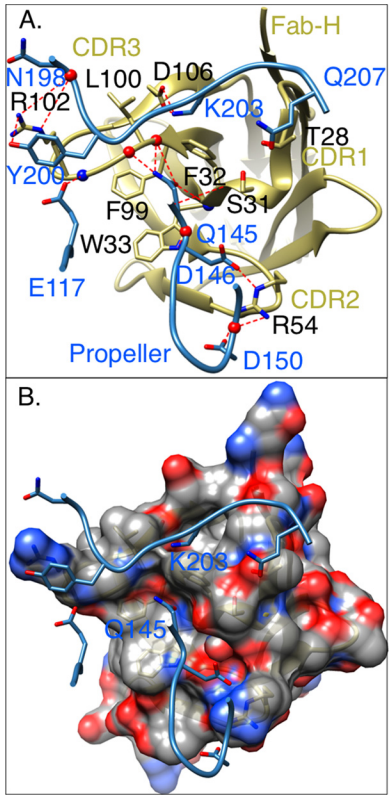

FIGURE 3. **αVβ3–17E6 Fab binding interface.** *A*, electrostatic and H-bond interactions at the αVβ3–17E6 Fab interface are represented with *dashed red lines*. Oxygens are in *red*, and nitrogens are in *blue*. Main chains are labeled and colored as in Fig. 2*A*. *B*, electrostatic potential surface of 17E6 Fab heavy chain at the integrin interface. Two adjacent pockets in Fab-H house human integrin residues Gln-145 and Lys-203. The orientation in *B* is the same as in *A*.

served Lys-203 for 17E6 interaction with αV was evaluated in a K203A mutation of human αV. K203A mutant αV did not affect folding of the integrin as assessed by surface binding of mAbs AP3 and 7E3 (Fig. 5*B*); however, it was no longer recognized by 17E6 Fab (Fig. 5*B*).

Molecular Dynamic Simulation of αVβ3–17E6 Interaction Supports the Structural and Mutational Data—The energy of interaction between the integrin αV Propeller and 17E6 Fab was simulated for wild-type Propeller, K203A, and Q145D/K145N mutants (Fig. 5*C*). The energy of interaction for wild-type Propeller fluctuated at ~500 kCal/mol, but K203A showed an abrupt energy drop to ~300 kCal/mol within ~0.2 ns after initiation of the simulation, reflecting loss of the salt bridge between Lys-203 and Asp-106_{H3}.

The Lys-203–Asp-106_{H3} bond distance in the Q145D/K145N αV mutant yielded a minimum distance of ~2.5 Å as in wild type during equilibration but showed much larger fluctuations, reflecting less stable binding (Fig. 5*D*). The energy of interaction of Q145D/K145N with 17E6 Fab dropped, first to ~450 kCal/mol then to ~300 kCal/mol. Initially, the Asp-146–Arg-54_{H2} bond disappeared in Q145D/K145N structure, replaced by Asp-148 and Asp-150 bonds with Arg-54_{H2} (Fig. 5*E*). These bonds, as well as a Lys-145–Phe-99 H-bond, were lost at 10–12 ns, with a simultaneous reduction in the energy of interaction between the Q145D/K145N Propeller and 17E6 Fab to ~300 kCal/mol (Fig. 5*C*).

Inserting the average interaction energies over the last 10 ns of simulations for wild-type (−478 kCal/mol), K203A (−338 kCal/mol), and Q145K/D146N (−292 kCal/mol) Propeller into Equation 3 yielded association constant ratios of 2×10^{-99} for

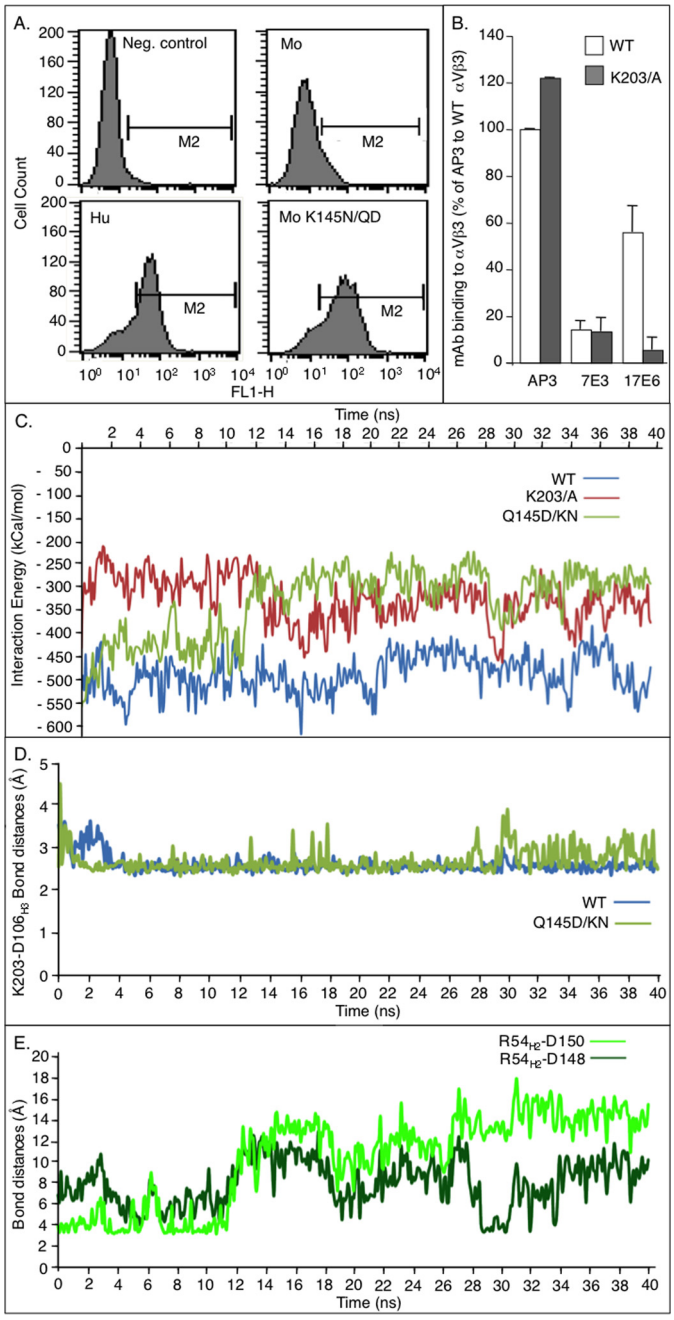

FIGURE 5. **Biochemical and computational validation of αVβ3–17E6 binding interface.** *A*, flow cytometric analysis of 17E6-stained mouse 3T3 cells expressing mouse (*Mo*) or human (*Hu*) αVβ3, as well as 3T3 expressing K145N/Q145D chimeric murine αV paired with endogenous mouse β-chains. Negative (*Neg.*) control represents 3T3 staining with the secondary antibody only. *B*, histograms (means ± S.D.) of two (for AP3) and of three (for the others) independent experiments, showing binding of AP3 IgG, 7E3 Fab, and 17E6 Fab to K562 stably expressing full-length human WT or mutant (K203A) αVβ3. *C*, computed interaction energy between 17E6 Fab and the wild-type, K203A, and Q145D/K145N Propeller domain. *D*, computed bond distances between Lys-203 and Asp-106$_{H3}$ in the wild-type and Q145D/K145N Propeller. *E*, computed bond distances between Arg-54$_{H2}$ and Asp-150 and Asp-148 that form as a result of the D146N mutation in the Propeller.

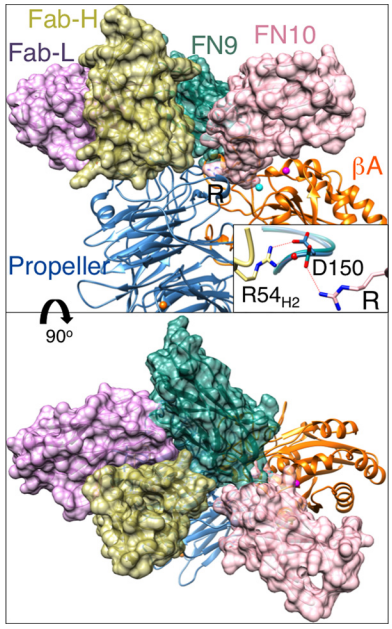

FIGURE 6. **Model of FN-bound αVβ3–17E6 complex.** Superposition of the Propeller domains from αVβ3-FN10 complex (Protein Data Bank code mmx4) and αVβ3–17E6 Fab structures. FN9 (from FN9–10 NMR structure (Protein Data Bank code 2mfn; model 4.7) docked onto FN10 of Protein Data Bank code mmx4 is also shown. FN10 (in *pink*), FN9 (*deep cyan*), and the heavy (*H*, in *dark khaki*) and light (*L*, in *plum*) chains of 17E6 Fab chain are surface-rendered. One of the four metal ions at the base of the Propeller is shown (*orange sphere*). The MIDAS metal ion (*cyan sphere*) from Protein Data Bank code mmx4 and ADMIDAS (*magenta sphere*) of αVβ3–17E6 Fab are shown. The Arg side chain of the ligand FN10 is shown. *Inset*, orientation of Asp-150 side chain in αVβ3–17E6 and αVβ3-FN10 crystal structures. Asp-150 forms a salt bridge (*red dotted line*) with ligand Arg in αVβ3-FN10: this is absent in αVβ3–17E6 because of the Asp-150–Arg-54$_H$ contacts. Side chains are shown as *sticks* with nitrogens in *blue* and oxygens in *red*. The *lower image* represents a 90° clockwise rotation of the *upper image*.

K203A, and 8×10^{-132} for Q145D/K145N. Thus either Propeller mutation markedly reduced affinity of 17E6, despite maintenance of other ionic and van der Waals bonds between the two interactants. The above biochemical and computational studies thus verify the structural model and underscore the critical roles of Gln-145 → Asp and Lys-203 in 17E6 recognition of human αVβ3.

Impact of Bound 17E6 Fab on Fibronectin Binding to Cellular αVβ3—Superimposition of the αVβ3–17E6 Fab structure onto that of αVβ3-FN10 structure (Protein Data Bank code 4mmx),[3] predicts that no clashes would occur between bound 17E6-Fab and FN10 (Fig. 6). In RGD-bound αVβ3 structures (35), the ligand Arg inserts into a pocket in the Propeller domain and is stabilized by salt bridges to OD1 and OD2 of Asp-218 and to OD1 of Asp-150. In αVβ3–17E6 Fab structure, stability of the ligand Arg in the Propeller pocket is predicted to be weakened by loss of the salt bridge to Asp-150, which contacts Arg-54$_{H2}$ instead (Fig. 6, *top panel*, *inset*). Furthermore, docking FN10 from each of 10 nuclear magnetic resonance structures of the FN9–10 fragment (Protein Data Bank code 2mfn) onto that of FN10 in the superimposed αVβ3-FN10 and αVβ3–17E6 structures suggested that FN9 would clash mainly with the light chain of bound 17E6 Fab, even when the least conflicting FN9–10 model (model 4.7) was used (Fig. 6). This predicted that binding of FN9–10 to cellular αVβ3 would be inhibited by 17E6 Fab. This was tested experimentally. Binding of soluble fluoresceinated FN10 and FN9–10 to full-length αVβ3 stably expressed on K562 cells was measured in presence or absence of unlabeled 17E6 Fab. 17E6 Fab reduced binding of FN10 to

[3] J. F. Van Agthoven, *et al.*, unpublished observations.

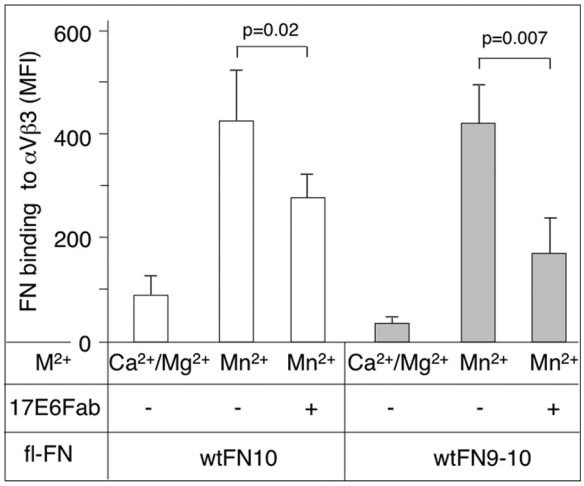

FIGURE 7. **Effect of 17E6 on binding of FN to αVβ3.** Histograms (mean ± S.D.; $n = 3$) show relative binding of Alexa Fluor 488-labeled FN10 or FN9–10 (*fl-FN*) to αVβ3 stably expressed on K562, measured by flow cytometry. *p* values are shown above the histograms. Binding was carried out in 1 mM of Ca^{2+}/plus 1 mM Mg^{2+} or 1 mM Mn^{2+} in the absence (−) or presence (+) of unlabeled 17E6 Fab.

Mn^{2+}-activated cellular αVβ3 by some 40% and that of FN9–10 by some 60% (Fig. 7).

DISCUSSION

In this report, we describe the first crystal structure of an integrin ectodomain complexed to a function-blocking mAb, the Fab fragment of 17E6, in presence of Mn^{2+}, an integrin-activating cation. The new structure allowed an atomic level analysis of the αVβ3–17E6 interface. It showed that 17E6 exclusively contacted the αV Propeller domain and did so at those critical residues on blades 2 and 3 that precisely correspond to the demonstrated phylogenetic specificity of inhibition of 17E6. The binding site reveals a mechanism by which 17E6, which itself lacks an RGD sequence, allosterically inhibits RGD-based ligand interaction with cellular αV integrins.

The integrin in the complex assumes a bent conformation and also in solution, suggesting that the well established integrin activator Mn^{2+} does not necessarily switch the αVβ3 ectodomain to a linear conformation as has been suggested (36). This finding is consistent with our earlier fluorescent lifetime imaging study revealing a bent 17E6-bound cellular αVβ3 in Mn^{2+} (15) and a cryoelectron tomography study showing no dramatic genu extension upon Mn^{2+}-induced activation of membrane-bound unliganded αIIbβ3 integrin (37). It could be argued that binding of 17E6 prevents Mn^{2+}-induced conformational switching of αVβ3. This seems unlikely, because 17E6 Fab bound to αVβ3 did not block an increase in hydrodynamic radius of the ectodomain complex triggered by a cyclic RGD ligand. Furthermore, binding of 17E6 did not block a subsequent Mn^{2+}-induced expression of a conformation-dependent LIBS (15). We also found that despite the crystallization of the αVβ3-Fab complex in the presence of 5 mM $MnCl_2$, only ADMIDAS but neither MIDAS nor LIMBS of αVβ3 were occupied by a metal ion. However, all three sites were occupied by Mn^{2+} when αVβ3 was bound by an RGD ligand (35), suggesting that the latter appears necessary for stable coordination of the metal ion at MIDAS and LIMBS in αVβ3.

The αVβ3 ectodomain from the complex was superimposable on unliganded αVβ3 (Protein Data Bank code 3ije) (15), yielding a Cα root mean square deviation of 3.44 Å. This improved to 1.53 Å when superimposition excluded Calf-1/2 and βTD domains, which gave a root mean square deviation of 4.31 Å in such an alignment. Conversely, superimposition of Calf-1/2 and βTD domains exclusive of the rest of the integrin domains in the two structures gave a root mean square deviation of 1.53 Å. These data suggest that a rigid body movement of Calf-1/2 plus βTD differentiated the two structures. The origin of this movement is likely the different crystal contacts from symmetry-related molecules in the two structures of 17E6-bound *versus* unliganded αVβ3. The αVβ3–17E6 Fab structure, compared with the unliganded αVβ3 structure, lacks a major stabilizing area of interaction (595 $Å^2$) involving Calf-2 with the Propeller from a symmetry-related molecule. However, at the top of Calf-1, including the α-genu, it does have an interaction (207 $Å^2$) with the L-chain from a symmetry-related molecule. These differences likely account for the higher mobility of the Calf-1/2-βTD domains in the αVβ3–17E6 complex, allowing only a partial assignment of their side chains in the present structure. The higher mobility and/or the crystal contact Calf-1 makes with the symmetry-related molecule may also account for a lack of a visible metal ion at the α-genu.

17E6 recognizes the αV subunit only in human and primate integrins (10, 38, 39). Using αV-α5 chimeric subunits expressed as heterodimers with β1 on viable Chinese hamster ovary cells, Mould *et al.* (40) mapped the 17E6-binding site in human integrin αV to Propeller residues Ala-107–Trp-226. We found that this region, which is identical in sequence to that in rodents except for a K145N substitution of human residues Q145D, contains all the residues that directly contact 17E6 Fab. Binding of 17E6 to chimeric αV/α5 in which the αV sequence Gln-145–Asp–Ile–Asp–Ala–Asp was replaced with the corresponding sequence Asp-154–Phe–Ser–Trp–Ala–Ala from integrin α5 subunit (40) indicated that Gln-145 is the critical residue accounting for primate specificity and that it could be replaced by an Asp but not a Lys (as in the rodent sequence). This interpretation is consistent both with the crystal structure and with mutational analysis. In the crystal, an Asp replacing Gln-145 could form the same H-bonds with the carbonyl oxygens of Phe-99 and Leu-100 and the amide main chain of Trp-33. In cells, we could show that replacing murine Lys-145 → Asn with human Gln-145 → Asp in αV was a gain of function mutation for 17E6 binding to mouse αV. Interestingly, excepting primates, this pair of residues is also substituted in those many other species, where cell adhesion, as we show here, is not inhibited by 17E6.

How does mAb 17E6 impair ligand binding to αVβ3? Superimposing the NMR structures of wild-type FN9–10 onto FN10 docked into the αVβ3–17E6 Fab complex predicted a significant clash of FN9 mainly with the light chain of 17E6, which would hinder binding of soluble FN9–10 to cellular αVβ3. Binding inhibition studies supported this prediction, showing ~60% reduction of FN9–10 binding when 17E6 was bound to cellular αVβ3. FN9, although unnecessary for binding of FN to αVβ3 (41), may yet clash with bound 17E6, thus reducing binding of FN9–10. The known flexibility of the FN9–10 interdo-

main linkage (42, 43) may explain why inhibition of binding of FN9–10 to cellular αVβ3 by 17E6 is not complete. The modest size of the αVβ3/FN10 interface seen in the crystal structure of this complex[3] may make it particularly susceptible to allosteric inhibition.

Mutating Asp-150 in the αV Propeller domain to alanine (Asp-150 → Ala) has been shown to reduce binding of the RGD-containing ligand-mimetic WOW-1 Fab to cellular αVβ3 by 37% (44). Our findings show that 17E6 Fab caused a 41% inhibition of binding of soluble RGD-containing FN10 to cellular αVβ3. This reduction may be explained by the predicted loss of the salt bridge Asp-150 normally makes with the ligand Arg. Thus 17E6-bound αVβ3 appears to functionally behave like the described Asp-150 → Ala αVβ3 mutant (44).

In addition to the inhibition of soluble ligand binding to cellular αVβ3 by monovalent 17E6, divalent 17E6 reduces the number of cell surface αVβ3 receptors through internalization, which may also contribute to the inhibition of cell adhesion by divalent 17E6 *in vitro* (11) and retarded growth of model melanoma in nude mice (10). Finally, integrin clustering by multivalent physiological ligands likely orients the integrin in the membrane into ordered arrays, which then encourage the formation of signal transduction complexes (45). Dimerization of αVβ3 by divalent 17E6 may interfere with such ordering of the liganded integrin in the membrane, destabilizing αVβ3-substrate interactions, altering signal transduction, and contributing to a greater effectiveness of divalent *versus* monovalent 17E6 in blocking cell adhesion.

Integrins are appealing therapeutic targets (46). The structure of αVβ3–17E6 Fab complex reveals the detailed inhibitory interactions between this mAb and its epitope. Changes might be engineered to productively modify the antibody-integrin interaction and potentially be used to guide development of novel therapeutics targeting related regions in other integrins. Because the 17E6 epitope is distinct from the ligand-binding MIDAS face of the β-subunit, perhaps 17E6 in combination with ligand mimetic drugs might achieve synergistic or additive therapeutic effects.

Acknowledgments—We thank H. P. Erickson for providing the FN7-10 plasmid, Dr. Rongguang Zhang and the staff at Beamline 19ID of the Argonne National Laboratory for assistance with data collection, and Zhiping Ding, Dirk Mueller-Pompalla, Catherine Eichhorn, and Melanie Pösser for expert technical assistance.

REFERENCES

1. Hynes, R. O. (2002) Integrins: bidirectional, allosteric signaling machines. *Cell* **110,** 673–687
2. Arnaout, M. A., Goodman, S. L., and Xiong, J. P. (2007) Structure and mechanics of integrin-based cell adhesion. *Curr. Opin. Cell Biol.* **19,** 495–507
3. Rodius, S., Chaloin, O., Moes, M., Schaffner-Reckinger, E., Landrieu, I., Lippens, G., Lin, M., Zhang, J., and Kieffer, N. (2008) The talin rod IBS2 α-helix interacts with the β3 integrin cytoplasmic tail membrane-proximal helix by establishing charge complementary salt bridges. *J. Biol. Chem.* **283,** 24212–24223
4. Hato, T., Pampori, N., and Shattil, S. J. (1998) Complementary roles for receptor clustering and conformational change in the adhesive and signaling functions of integrin αIIbβ3. *J. Cell Biol.* **141,** 1685–1695
5. Weis, S. M., and Cheresh, D. A. (2011) αv integrins in angiogenesis and cancer. *Cold Spring Harb. Perspect. Med.* **1,** a006478
6. Max, R., Gerritsen, R. R., Nooijen, P. T., Goodman, S. L., Sutter, A., Keilholz, U., Ruiter, D. J., and De Waal, R. M. (1997) Immunohistochemical analysis of integrin αvβ3 expression on tumor-associated vessels of human carcinomas. *Int. J. Cancer* **71,** 320–324
7. McCabe, N. P., De, S., Vasanji, A., Brainard, J., and Byzova, T. V. (2007) Prostate cancer specific integrin αvβ3 modulates bone metastatic growth and tissue remodeling. *Oncogene* **26,** 6238–6243
8. Lorger, M., Krueger, J. S., O'Neal, M., Staflin, K., and Felding-Habermann, B. (2009) Activation of tumor cell integrin αvβ3 controls angiogenesis and metastatic growth in the brain. *Proc. Natl. Acad. Sci. U.S.A.* **106,** 10666–10671
9. Albelda, S. M., Mette, S. A., Elder, D. E., Stewart, R., Damjanovich, L., Herlyn, M., and Buck, C. A. (1990) Integrin distribution in malignant melanoma: association of the β3 subunit with tumor progression. *Cancer Res.* **50,** 6757–6764
10. Mitjans, F., Sander, D., Adán, J., Sutter, A., Martinez, J. M., Jäggle, C. S., Moyano, J. M., Kreysch, H. G., Piulats, J., and Goodman, S. L. (1995) An anti-α v-integrin antibody that blocks integrin function inhibits the development of a human melanoma in nude mice. *J. Cell Sci.* **108,** 2825–2838
11. Castel, S., Pagan, R., García, R., Casaroli-Marano, R. P., Reina, M., Mitjans, F., Piulats, J., and Vilaró, S. (2000) αv integrin antagonists induce the disassembly of focal contacts in melanoma cells. *Eur. J. Cell Biol.* **79,** 502–512
12. Castel, S., Pagan, R., Mitjans, F., Piulats, J., Goodman, S., Jonczyk, A., Huber, F., Vilaró, S., and Reina, M. (2001) RGD peptides and monoclonal antibodies, antagonists of α_v-integrin, enter the cells by independent endocytic pathways. *Lab. Invest.* **81,** 1615–1626
13. Xiong, J. P., Stehle, T., Diefenbach, B., Zhang, R., Dunker, R., Scott, D. L., Joachimiak, A., Goodman, S. L., and Arnaout, M. A. (2001) Crystal structure of the extracellular segment of integrin α Vβ3. *Science* **294,** 339–345
14. Artoni, A., Li, J., Mitchell, B., Ruan, J., Takagi, J., Springer, T. A., French, D. L., and Coller, B. S. (2004) Integrin β3 regions controlling binding of murine mAb 7E3: implications for the mechanism of integrin αIIbβ3 activation. *Proc. Natl. Acad. Sci. U.S.A.* **101,** 13114–13120
15. Xiong, J. P., Mahalingham, B., Alonso, J. L., Borrelli, L. A., Rui, X., Anand, S., Hyman, B. T., Rysiok, T., Müller-Pompalla, D., Goodman, S. L., and Arnaout, M. A. (2009) Crystal structure of the complete integrin αVβ3 ectodomain plus an α/β transmembrane fragment. *J. Cell Biol.* **186,** 589–600
16. Dechantsreiter, M. A., Planker, E., Mathä, B., Lohof, E., Hölzemann, G., Jonczyk, A., Goodman, S. L., and Kessler, H. (1999) *N*-Methylated cyclic RGD peptides as highly active and selective $\alpha_V\beta_3$ integrin antagonists. *J. Med. Chem.* **42,** 3033–3040
17. Adair, B. D., Xiong, J. P., Maddock, C., Goodman, S. L., Arnaout, M. A., and Yeager, M. (2005) Three-dimensional EM structure of the ectodomain of integrin αVβ3 in a complex with fibronectin. *J. Cell Biol.* **168,** 1109–1118
18. Otwinowski, Z., and Minor, W. (1997) Processing of x-ray diffraction data collected in oscillation mode. *Methods in Enzymol.* **276,** 307–326
19. Storoni, L. C., McCoy, A. J., and Read, R. J. (2004) Likelihood-enhanced fast rotation functions. *Acta Crystallogr. D Biol. Crystallogr.* **60,** 432–438
20. Schröder, G. F., Levitt, M., and Brunger, A. T. (2010) Super-resolution biomolecular crystallography with low-resolution data. *Nature* **464,** 1218–1222
21. Brünger, A. T., Adams, P. D., Clore, G. M., DeLano, W. L., Gros, P., Grosse-Kunstleve, R. W., Jiang, J. S., Kuszewski, J., Nilges, M., Pannu, N. S., Read, R. J., Rice, L. M., Simonson, T., and Warren, G. L. (1998) Crystallography & NMR system: A new software suite for macromolecular structure determination. *Acta Crystallogr. D Biol. Crystallogr.* **54,** 905–921
22. Adams, P. D., Afonine, P. V., Bunkóczi, G., Chen, V. B., Davis, I. W., Echols, N., Headd, J. J., Hung, L. W., Kapral, G. J., Grosse-Kunstleve, R. W., McCoy, A. J., Moriarty, N. W., Oeffner, R., Read, R. J., Richardson, D. C., Richardson, J. S., Terwilliger, T. C., and Zwart, P. H. (2010) PHENIX: a comprehensive Python-based system for macromolecular structure solution. *Acta Crystallogr. D. Biol. Crystallogr.* **66,** 213–221
23. Jones, T. A., Zou, J. Y., Cowan, S. W., and Kjeldgaard. (1991) Improved

methods for building protein models in electron density maps and the location of errors in these models. *Acta Crystallogr. A* **47,** 110–119
24. Emsley, P., and Cowtan, K. (2004) Coot: model-building tools for molecular graphics. *Acta Crystallogr. D. Biol. Crystallogr.* **60,** 2126–2132
25. Pettersen, E. F., Goddard, T. D., Huang, C. C., Couch, G. S., Greenblatt, D. M., Meng, E. C., and Ferrin, T. E. (2004) UCSF Chimera: a visualization system for exploratory research and analysis. *J. Comput. Chem.* **25,** 1605–1612
26. Ludtke, S. J., Baldwin, P. R., and Chiu, W. (1999) EMAN: semiautomated software for high-resolution single-particle reconstructions. *J. Struct. Biol.* **128,** 82–97
27. Adair, B. D., Xiong, J. P., Alonso, J. L., Hyman, B. T., and Arnaout, M. A. (2013) EM structure of the ectodomain of integrin CD11b/CD18 and localization of its ligand-binding site relative to the plasma membrane. *PLoS One* **8,** e57951
28. Gupta, V., Gylling, A., Alonso, J. L., Sugimori, T., Ianakiev, P., Xiong, J. P., and Arnaout, M. A. (2007) The β-tail domain (βTD) regulates physiologic ligand binding to integrin CD11b/CD18. *Blood* **109,** 3513–3520
29. Phillips, J. C., Braun, R., Wang, W., Gumbart, J., Tajkhorshid, E., Villa, E., Chipot, C., Skeel, R. D., Kalé, L., and Schulten, K. (2005) Scalable molecular dynamics with NAMD. *J. Comput. Chem.* **26,** 1781–1802
30. Mehrbod, M., Trisno, S., and Mofrad, M. R. (2013) On the activation of integrin αIIbβ3: outside-in and inside-out pathways. *Biophys. J.* **105,** 1304–1315
31. Mehrbod, M., and Mofrad, M. R. (2013) Localized lipid packing of transmembrane domains impedes integrin clustering. *PLoS Comput. Biol.* **9,** e1002948
32. Chen, W., Lou, J., Hsin, J., Schulten, K., Harvey, S. C., and Zhu, C. (2011) Molecular dynamics simulations of forced unbending of integrin $\alpha_v\beta_3$. *PLoS Comput. Biol.* **7,** e1001086
33. Krautler, V., Van Gunsteren, W. F., and Hunenberger, P. H. (2001) A fast SHAKE: algorithm to solve distance constraint equations for small molecules in molecular dynamics simulations. *J. Comput. Chem.* **22,** 501–508
34. Guex, N., and Peitsch, M. C. (1997) SWISS-MODEL and the Swiss-Pdb-Viewer: an environment for comparative protein modeling. *Electrophoresis* **18,** 2714–2723
35. Xiong, J. P., Stehle, T., Zhang, R., Joachimiak, A., Frech, M., Goodman, S. L., and Arnaout, M. A. (2002) Crystal structure of the extracellular segment of integrin αVβ3 in complex with an Arg-Gly-Asp ligand. *Science* **296,** 151–155
36. Takagi, J., and Springer, T. A. (2002) Integrin activation and structural rearrangement. *Immunol. Rev.* **186,** 141–163
37. Ye, F., Liu, J., Winkler, H., and Taylor, K. A. (2008) Integrin αIIbβ3 in a membrane environment remains the same height after Mn^{2+} activation when observed by cryoelectron tomography. *J. Mol. Biol.* **378,** 976–986
38. Kraft, S., Diefenbach, B., Mehta, R., Jonczyk, A., Luckenbach, G. A., and Goodman, S. L. (1999) Definition of an unexpected ligand recognition motif for αvβ6 integrin. *J. Biol. Chem.* **274,** 1979–1985
39. Marshall, J. F., Rutherford, D. C., McCartney, A. C., Mitjans, F., Goodman, S. L., and Hart, I. R. (1995) αvβ1 is a receptor for vitronectin and fibrinogen, and acts with α5β1 to mediate spreading on fibronectin. *J. Cell Sci.* **108,** 1227–1238
40. Mould, A. P., Askari, J. A., and Humphries, M. J. (2000) Molecular basis of ligand recognition by integrin α5β1. I. Specificity of ligand binding is determined by amino acid sequences in the second and third NH_2-terminal repeats of the α subunit. *J. Biol. Chem.* **275,** 20324–20336
41. Bowditch, R. D., Hariharan, M., Tominna, E. F., Smith, J. W., Yamada, K. M., Getzoff, E. D., and Ginsberg, M. H. (1994) Identification of a novel integrin binding site in fibronectin. Differential utilization by β3 integrins. *J. Biol. Chem.* **269,** 10856–10863
42. Baron, M., Main, A. L., Driscoll, P. C., Mardon, H. J., Boyd, J., and Campbell, I. D. (1992) ^{1}H NMR assignment and secondary structure of the cell adhesion type III module of fibronectin. *Biochemistry* **31,** 2068–2073
43. Copié, V., Tomita, Y., Akiyama, S. K., Aota, S., Yamada, K. M., Venable, R. M., Pastor, R. W., Krueger, S., and Torchia, D. A. (1998) Solution structure and dynamics of linked cell attachment modules of mouse fibronectin containing the RGD and synergy regions: comparison with the human fibronectin crystal structure. *J. Mol. Biol.* **277,** 663–682
44. Honda, S., Kashiwagi, H., Kiyoi, T., Kato, H., Kosugi, S., Shiraga, M., Kurata, Y., and Tomiyama, Y. (2004) Amino acid mutagenesis within ligand-binding loops in α v confers loss-of-function or gain-of-function phenotype on integrin αvβ3. *Thromb. Haemost.* **92,** 1092–1098
45. Friedland, J. C., Lee, M. H., and Boettiger, D. (2009) Mechanically activated integrin switch controls α5β1 function. *Science* **323,** 642–644
46. Goodman, S. L., and Picard, M. (2012) Integrins as therapeutic targets. *Trends Pharmacol. Sci.* **33,** 405–412